Spectroscopic ellipsometry study of $Cu_2ZnSn(S_xSe_{1-x})_4$ bulk polycrystals

Sergiu Levcenko[a], Elena Hajdeu-Chicarosh[b,g,*], Rosalía Serna[c], Maxim Guc[b,d], Ivan A. Victorov[e], Alexandr Nateprov[b], Ivan V. Bodnar[e], Raquel Caballero[f], José Manuel Merino[f], Ernest Arushanov[b] and Máximo León[f]

[a]*Department Structure and Dynamics of Energy Materials, Helmholtz-Zentrum Berlin fur Materialien und Energie, Hahn-Meitner-Platz, D-14109 Berlin, Germany*

[b]*Institute of Applied Physics, Academy of Sciences of Moldova, Academiei 5, MD 2028 Chisinau, Moldova*

[c]*Laser Processing Group, Instituto de Optica, IO, CSIC, Serrano 121, 28006 Madrid, Spain*

[d]*IREC, Catalonia Institute for Energy Research, C. Jardins de les Dones de Negre 1, 08930 Sant Adria del Besos (Barcelona), Spain*

[e]*Belarusian State University of Informatics and Radioelectronics, P. Brovka 6, 220013 Minsk, Belarus*

[f]*Department of Applied Physics M12, Universidad Autonoma de Madrid, C/Francisco Tomas y Valiente 7, 28049 Madrid, Spain*

[g]*SunGa Ltd., Bolgarscaia 87, MD 6101 Ceadir-Lunga, Moldova*

**Corresponding author: elenahajdeu@yahoo.com, +373 22 735531*

Abstract

The pseudo dielectric function of $Cu_2ZnSn(S_xSe_{1-x})_4$ [x = 0.35, 0.62, 0.81] bulk polycrystals is determined over the range 1.1 – 4.6 eV at room temperature from the analysis of spectroscopic ellipsometry data using the Adachi model. From the analysis, the lowest E_0 transition and high energy E_{1A} and E_{1B} transitions are clearly identified, and used to follow the evolution of the pseudo dielectric function as a function of the composition. It is shown that the fundamental E_0 and high energy E_{1A} transitions can be tuned by increasing the sulfur content over a range of 0.3 eV. These results show the potential of the kesterite compounds for the design of efficient tailored photovoltaic solar cells.

Keywords: ellipsometry, polycrystals, kesterites, semiconductor compounds, optical spectroscopy, Raman spectroscopy.

1. Introduction

Although $Cu_2ZnSn(S,Se)_4$ kesterite semiconductors exhibit an optimum band gap for profiting of the solar spectrum, a high absorption coefficient, and are composed by earth-abundant elements, however the photovoltaic devices based on them have not yet achieved the attractive efficiencies to replace CdTe or $Cu(In,Ga)Se_2$-based thin film devices. One of the fundamental limitations of the kesterite materials is the large amount of the intrinsic defects, which considerably limits the further increase in efficiency [1-3]. Chen et al. [4] have compared the properties of the defects in Cu_2ZnSnS_4 (CZTS) and $Cu_2ZnSnSe_4$ (CZTSe) and found that the negative effects of the deep defects are much stronger in sulfides than in selenides. Some recent studies have shown that the Sulfur (S) substitution with Selenium (Se) in the $Cu_2ZnSn(S_xSe_{1-x})_4$ (CZTSSe) compounds, where x varies from 0 to 1, an adjustment of the bandgap, and therefore of the physical properties of these compounds, can be obtained [5-8]. This has resulted in a promising efficiency of CZTSSe solar cells up to 12.6 % [5], which has been largely achieved due to the optimization of the thin film coating methods and to the optical architecture of the photovoltaic device structure. Therefore, the next step in order to increase the efficiency of the solar absorbers based on CZTSSe semiconductors should be the fundamental study of their intrinsic properties with the aim to understand and to minimize all the detrimental effects. At the moment there are only few studies referring to the Raman [2,6,8-10], structural [2,7,11] and optical properties [3,5,12-16], including a comprehensive study on the optical properties of kesterite $Cu_2ZnSn(S_xSe_{1-x})_4$ with intermediate sulfur content ($0.2<x<0.4$) [13]. This last study was conducted by combining both experimental (spectroscopic ellipsometry (SE) on CZTSSe thin film absorbers) and theoretical (*ab initio* calculations) methods that led to the determination of the dielectric functions, bandgaps E_g and critical points (CP) transition energies E_0 and E_1 [13]. However, these results are not enough for a detailed characterization of these complex solid solutions. To compare different experimental results, it should be kept in mind that, the optical response of the thin film has been often treated using the multi-layer stack model [13,14] which has a limited accuracy. The multi-layer stack approach can be avoided by measuring the optical response on bulk polycrystals. Besides, the results from this type of measurements are also relevant for the design of actual solar cell devices, where a polycrystalline material is used.

This work aims to study the optical properties of high quality $Cu_2ZnSn(S_xSe_{1-x})_4$ polycrystals with x = 0.35, 0.62 and 0.81 prepared by the Bridgman method, by using SE in a wide spectral range from 1.1 to 4.6 eV. A combined analysis by Energy Dispersive X-ray microanalysis (EDX) and Raman

spectroscopy of the samples used for this study has been performed in order to assess their compositional and structural (crystalline phases) properties. Based on the experimental findings, we propose a dielectric function model that can be extended to the full compositional range [$0 \leq x \leq 1$].

2. Experimental details

$Cu_2ZnSn(S_xSe_{1-x})_4$ polycrystals were grown by the modified Bridgman method through the direct synthesis from stoichiometric quantities of high purity (> 99.999%) Cu, Zn, Sn, S and Se and sealed in double silica ampoules at a pressure of 10^{-3} Pa. The material was heated at 50 K/h to about 870 K and then up to 1280 K with a 2 h annealing at both temperatures, with the vibration connected. Then the vibration was switched off and an oriented crystallization of the melt was carried out, lowering the temperature of the furnace at a rate of ~ 2 K/h to ~ 1020 K, annealing during 600 h at this temperature for homogenization purposes of the ingots.

For the selected samples, chemical composition was measured by EDX measurements (Oxford instruments, model INCA Xsight) inside a Hitachi S-3000N scanning electron microscope. The composition measurements were performed on several sample points to determine the average composition for the ellipsometry analysis.

The formation of solid solution quaternary phases has been examined by Raman scattering technique because our previous studies have demonstrated that is a suitable technique to determine both the crystallinity of the samples and the possible presence of secondary phases [6,8,10,17]. These measurements are performed in a backscattering configuration using the Horiba Jobin Yvon iHR320 spectrometer coupled with a CCD detector. The spectra were excited by a YAG:Nd solid-state laser (532 nm) with a power of ~ 90 W/cm^2.

Optical spectra were recorded with a variable-angle spectroscopic ellipsometer (J.A. Woollam VASE) at room temperature in the photon energy range of 1.1 to 4.6 eV. The optical spectra acquired at incidence angles of 60°, 65° and 70° showed an isotropic response of the sample. Note that to minimize the effect of roughness and the residual oxides on the surface sample, a special treatment following the method of Albornoz et al. [18] was performed.

3. Theoretical background

It has been successfully demonstrated that the model for the dielectric function (MDF) of Adachi [19,20] can be used for description of the pseudo complex dielectric function $\varepsilon = \varepsilon_1 + i\varepsilon_2$, in the $Cu_2ZnSnSe_4$ and Cu_2ZnSnS_4 kesterite materials [17,21]. In particular, for the energy range from the

absorption onset up to about 4.6 eV, ε is composed of the contributions from the band gap transition, E_0 and high-energy $E_{1\beta}$ ($\beta = A, B$) transitions:

$$\varepsilon(E) = \varepsilon^{(0)}(E) + \varepsilon^{(1)}(E), \quad (1)$$

where E is the photon energy.

The $\varepsilon^{(0)}(E)$ term is given by:

$$\varepsilon^{(0)}(E) = AE_0^{-3/2}\chi_0^{-2}(2 - (1+\chi_0)^{1/2} - (1-\chi_0)^{1/2}) \quad (2)$$

where $\chi_0 = (E + i\Gamma_0)/E_0$, and A and Γ_0 are the strength and the broadening energy of the E_0 transition, respectively. The $\varepsilon^{(1)}(E)$ component is given by:

$$\varepsilon^{(1)}(E) = B_{1A}[1 - (E/E_{1A})^2 - i(E/E_{1A})\Gamma_{1A}]^{-1} - B_{1B}\chi_{1B}^{-2}\, ln(1 - \chi_{1B}^2) \quad (3)$$

where $B_{1\beta}$ ($\beta = A, B$), $\Gamma_{1\beta}$($\beta = A, B$) and E_β ($\beta = A, B$) are the strength, the broadening energy and energy value of the corresponding transition. Note, that E_{1A} (E_{1B}) transition are close to the 2D-M_1 (2D-M_0) CP's, respectively.

Since the Gaussian type broadening mechanisms are more likely than the Lorentzian ones which are implemented in the Eq. (2) and (3) for the interband transitions, we employ the general equitation suggested by Kim at al [22], as follows,

$$\Gamma_i'(E) = \Gamma_i \, exp\left(-s_i\left(\frac{E-E_i}{\Gamma_i}\right)^2\right) \quad (4)$$

where s_i is a non-dimensional parameter, Γ_i is the broadening parameter, E_i is the transition energy, and i subscript corresponds to 0, 1*A or* 1*B*.

The spectroscopic ellipsometry measurements describe the change in polarization that takes place when the light interacts with the sample surface, and this change is given by two experimental parameters delta (Δ_{exp}) and psi (Ψ_{exp}) as a function of the wavelength. These parameters represent respectively the change in the phase of the light (Δ_{exp}) and in the amplitude ratio between the p- and s- polarized light (Ψ_{exp}). They are related to the Fresnel reflection coefficients $\boldsymbol{r}_p$ and $\boldsymbol{r}_s$ for the p- and s-polarized light by the relationship $tan(\Psi_{exp})\, \boldsymbol{e}^{i\,\Delta exp} = |\boldsymbol{r}_p/\boldsymbol{r}_s|$ [23]. In order to determine the MDF parameters from the measured ellipsometry parameters Δ_{exp} and Ψ_{exp} we have considered a three-phase model [24] that is formed by air (incident media), a rough surface layer and the bulk material of the polycrystalline sample. The surface roughness has been modeled by a Bruggeman effective medium approximation (EMA) to describe its pseudo dielectric function by assuming a 50 % ratio of air voids and 50% bulk CZTSSe [25]. Finally, the simulated annealing (SA) algorithm [26] has been employed to perform a global minimization procedure of the following objective function [27]:

$$F = \sum_{i=1}^{N} \left(\left| \frac{\Delta(E_i)}{\Delta_{\exp}(E_i)} - 1 \right| + \left| \frac{\Psi(E_i)}{\Psi_{\exp}(E_i)} - 1 \right| \right)^2 \quad (5)$$

where $\Delta_{exp}(E_i)$, $\Psi_{exp}(E_i)$, and $\Delta(E_i)$, $\Psi(E_i)$ are the experimental and calculated values of the ellipsometry parameters Δ and Ψ at the E_i point, respectively, and N is the number of the experimental points.

4. Results and discussions

The composition of the areas selected for this study of the CZTSSe samples as determined by the EDX measurements is given in Table 1.

TABLE 1. *Composition of the CZTSSe polycrystals measured by EDX*

Sample	Cu, at.%	Zn, at.%	Sn, at.%	S, at.%	Se, at.%	Cu/(Zn+Sn)	Zn/Sn	S/(S+Se)
SeS3	25.6	12.2	12.8	39.9	9.5	1.02	0.97	0.81
Se2S2	25.5	12.0	12.8	30.6	19.1	1.03	0.94	0.62
Se3S	26.4	13.1	12.8	16.5	31.2	1.02	1.03	0.35

The Raman scattering spectra of the studied CZTSSe bulk crystals under different excitation wavelengths are shown in Figure 1. Figure 1a, obtained under 532 nm laser excitation, shows two spectral regions with broad and strongly overlapped peaks. According to previous studies [6,8] these regions are related to the vibration of selenium and sulfur atoms, or to the common sulfur-selenium vibrations. Additionally, a significant broadening of the peaks is an expectable effect in the solid solution systems [6,8,10]. The peaks were blue shifted with the increase of the S content and their relative integrated intensity yields the S/(S+Se) ratio [8], which was found to be close to the one measured by EDX (0.80 for SeS3 sample, 0.54 for Se2S2 sample and 0.32 for Se3S sample). The Raman measurements were also performed with a UV (325 nm) and NIR (785 nm) excitation wavelengths to exclude the possible presence of different secondary phases (an example of the spectra could be found in Figs. 1b and 1c). In none of the spectra measured in the analyzed regions of the samples were found the Raman peaks of secondary phases (like ZnS, SnS, CuS, SnSe, CuSe, Cu_2SnS_3 or Cu_2SnSe_3), which means that they are absent of or are present in negligible concentration. Moreover, the good agreement between the composition ratios of EDX and Raman analysis could be another additional criterion for the secondary phase absence. Indeed, the formation of minor secondary phases including only S or Se anions is hardly detected by EDX analysis, but will result in

a change in the real S/(S+Se) ratio in the kesterite compound, which will be reflected in the Raman spectra. Thus, the presence of secondary phases will result in different S/(S+Se) ratios measured by EDX and Raman spectroscopy, which is not the case of the present study. The ellipsometry spectra were measured in the same area of the samples as Raman spectra, thus no influence of the secondary phases is expected for the following analysis of optical parameters of CZTSSe solid solutions.

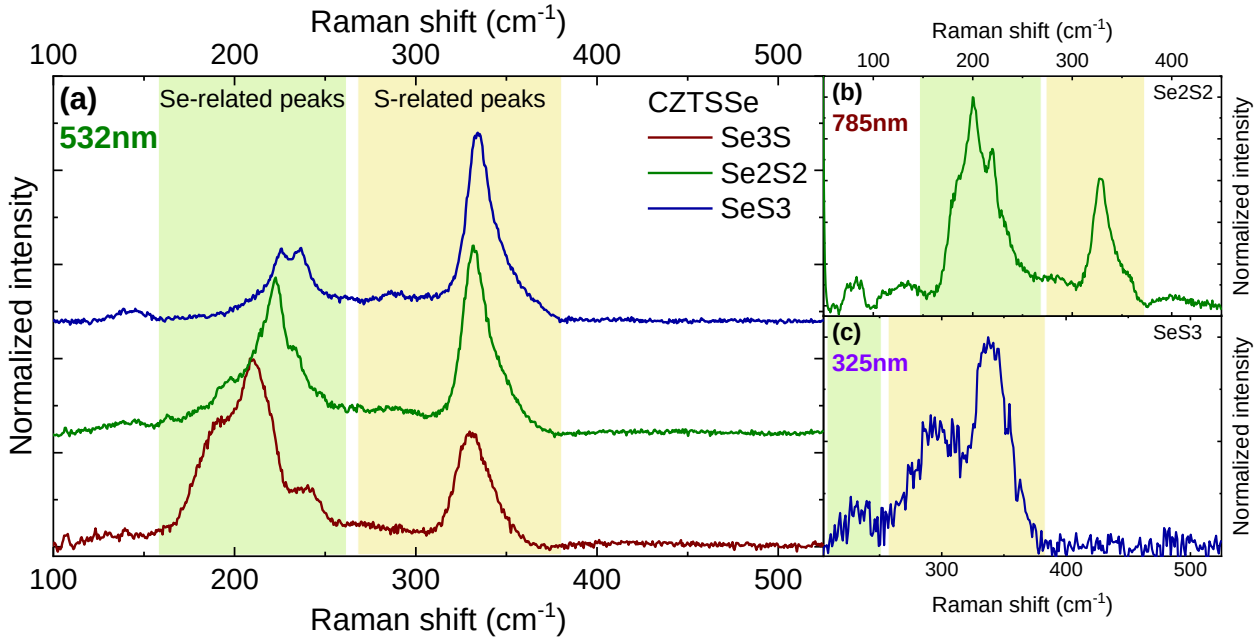

FIG. 1. *Raman scattering spectra of CZTSSe bulk crystals measured under different excitation wavelengths: 532, 785 and 325 nm.*

Figure 2 shows the comparison between the experimental ellipsometric curves (Δ_{exp}, Ψ_{exp}) and the calculated ones based on the Adachi model for samples Se3S, Se2S2 and SeS3. The calculated curves agree very well with the experimental ones, and the values of the relative errors are in the range 1 – 4 %. Table 2 summarizes the values of the MDF parameters, which were obtained from the minimizing routine (Eq. (5)). For the surface roughness layer, values in the range 7 – 9 nm were obtained, which are acceptable taking into account the surface preparation method used for the SE measurements. It should be noted that the relative difference between the experimental and the theoretical curves is slightly larger in the low energy region, especially in the range of 1~1.5 eV. These small differences, however, do not affect the accurate determination of fundamental band gap E_0 transition that can be linked to a clear change in slope, well identified in these curves. While there are might be some systematic errors in the measurements that are difficult to account [28], we assume that the observed deviations to be a consequence of the three phase model and contributions from the sub band gap absorption in kesterite. The former includes only one upper layer to describe the nonideal surfaces of the bulk polycrystals and the latter have been reported both for CZTS and CZTSe quaternary compounds. Although there is no broad consensus, the origin of

this absorption tail can be due to cation disorder [29]. The presence of these tail absorption states will not be discussed further in this work and we will focus on the main transitions.

According to the performed calculations, the Gaussian broadening mechanism is very small for the E_0 transition and therefore can be neglected. The high frequency dielectric constant, ε_∞, is directly related to the MDF strength parameters and is expressed by a simple relation of $\varepsilon_\infty \approx A/(4*E_0^{1.5}) + B_{1A} + B_{1B}$. The determined ε_∞ values are 8.03, 8.51, and 8.92 for the SeS3, Se2S2, and Se3S samples, respectively. With regard to the application of the CZTSSe thin film as an active absorber layer in the photovoltaic devices, we provide the pseudo complex optical constants such as the refractive index and extinction coefficient (Fig. 3(b)), as well as the normal incidence reflectivity and absorption coefficient (Figs. 3(c) and 3(d)).

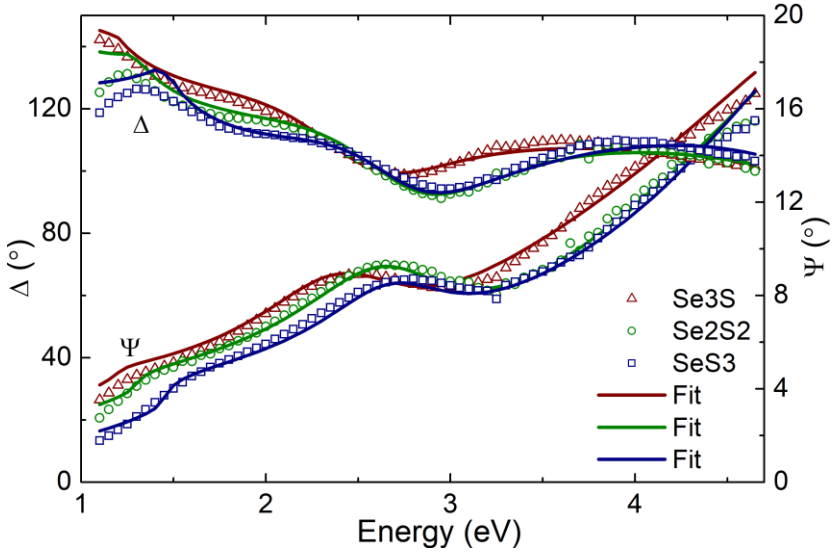

FIG. 2. *Experimental Ψ and Δ spectra at an incidence angle of 70º (points) and numerically calculated (solid lines) using three phase model (air, surface and bulk layers) for samples Se3S, Se2S2 and SeS3 of the CZTSSe polycrystals.*

Let us return to the interband transitions considered in the modelling of the pseudo dielectric function for CZTSSe samples. The E_0 transition is ascribed to the lowest transition between the valence band maximum (VBM) to the conduction band minimum (CBM) at the Γ(0,0,0) point in the Brillouin zone (BZ) [30,31]. The obtained results on the lowest transition, which varies from 1.2 to 1.5 eV with increasing the content of S (Table 2), are consistent with the earlier SE results on CZTSSe thin films and ab initio calculations [13]. A comparison between the results presented here on the E_0 transition with available literature data [13,17,21,31] will be further discussed below.

TABLE 2. *Model parameter values.*

Parameters / Samples	$A(eV^{1.5})$	$E_0(eV)$	$\Gamma_0(eV)$	B_{1A}	$E_{1A}(eV)$	Γ_{1A}	s_{1A}	B_{1B}	$E_{1B}(eV))$	$\Gamma_{1B}(eV)$	s_{1B}	Error Ψ%	Error Δ%
SeS3	4.3	1.47	0.02	0.4	2.69	0.27	0.04	6.9	4.67	0.5	0.03	3.5	2.2
Se2S2	2.7	1.32	0.03	0.6	2.66	0.31	0.03	7.4	4.79	0.5	0.13	3.6	1.3
Se3S	2.0	1.20	0.02	0.5	2.44	0.31	0.1	8.0	4.69	0.6	0.05	2.4	1.6

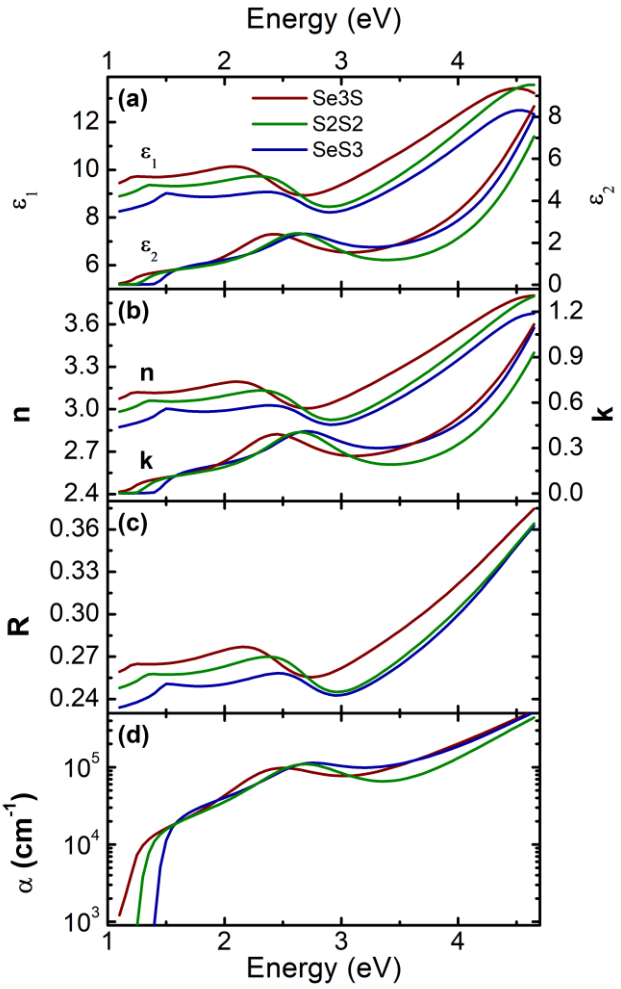

FIG. 3. *Numerically calculated (a) pseudo dielectric function ε (E) = ε1(E) +i ε2(E), (b) extinction coefficient, k, and refractive index, n, (c) normal-incidence reflectivity, R, and (d) absorption coefficient, α, by using the MDF model and the SA algorithm for the CZTSSe polycrystals.*

The higher E_{1A} transition observed in the range 2.4 – 2.7 eV for the CZTSSe samples can be attributed to the transition from the VBM to the second conduction band at Γ (0,0,0) point [30], or from the transitions at the P (1/2,1/2,1/2) point in the BZ [13]. It was found that E_{1A} transition is by 1.4 eV higher in energy than the band gap transition E_0 [13]. Our results are in agreement with these findings, but the shift of the E_{1A} with respect to the E_0 transition is smaller and is about 1.2 – 1.3 eV. Regarding the E_{1B} transition (at 4.7 – 4.8 eV) origin, which might contain numerous contributions from different

types of transitions occurring over a wide region of the BZ [32], it can be ascribed to transitions at Z(0,0,1) and Y1(1/2,1/2,-1) points in the BZ [13]. It should be noted that due to the spectral range limits in our SE measurements, the E_{1B} transition characteristics are less accurate, and higher energy data points are further needed to achieve precise values.

An important feature of the kesterite materials for photovoltaic applications consists in the possibility of fine-tuning the band gap values, E_g, by replacing S with Se. With this goal, different methods have been investigated to fabricate high quality CZTSSe thin films to be used as absorber material of solar cells [33,34]. The difficulty arises in creating the optimal S distribution though the kesterite layer to maximize the open circuit voltage V_{OC} and short circuit current I_{SC} that lead to an enhanced device efficiency. In Fig. 4, we show our data values for the E_0 transition as a function of the S content (x) together with previous results reported for the band gap for CZTSSe solid solutions [12,13,17,21].

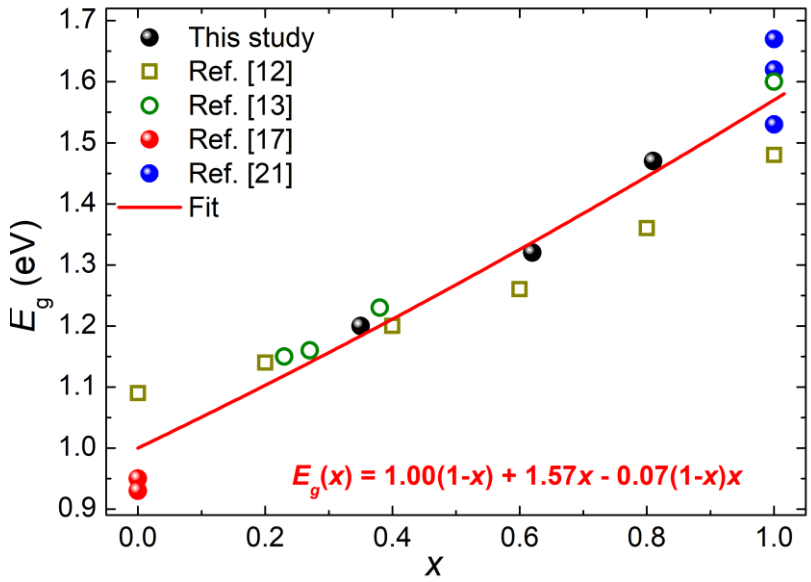

FIG. 4. *Band-gap energies of $Cu_2ZnSn(S_xSe_{1-x})_4$ solid solutions as a function of composition x.*

For instance, experimentally it is found an almost linear increase of the E_g values from ~ 1 to 1.55 eV [13], which is close to those calculated in Ref. [16] (~ 0.78 – 1.53 eV), but larger than those calculated in Ref. [9] (~ 0.27 – 0.87 eV) with increasing x. On the other hand, a stronger nonlinearity in the band gap increasing with x from 1.09 to 1.48 eV was experimentally obtained by the authors of Ref. [12] from absorption spectra measurements. Figure 4 shows the trend in E_g, which can be fitted to a parabolic form $E_g(x) = (1 - x)\, E_g(0) + xE_g(1) - b{\cdot}x(1 - x)$, where b is the bowing parameter [15]. It should be pointed out that all experimental points presented in the Fig.4 were used for the fitting procedure. Therefore, we have obtained a nonlinear increasing of E_g with increasing S content, with b value of ~ 0.07 eV, in line with the values of ~ 0.003 – 0.09 eV obtained in Ref. [15] or 0.08

obtained in Ref. [35]. We assume that these differences are due to the complexity of the solid solutions of CZTSSe and the strong dependence of the physical properties on the macroscopic state of the samples, composition, homogeneity and technological conditions of the sample growth.

5. Conclusions

In conclusion, we have reported the pseudo dielectric function of $Cu_2ZnSn(S_xSe_{1-x})_4$ bulk polycrystalline samples grown by the modified Bridgman method in the visible near-infrared range from 1.1 to 4.6 eV. The lowest E_0 transition and high energy E_{1A} and E_{1B} transitions are well resolved in the pseudo dielectric function spectra, allowing to propose a MDF Adachi model for the pseudo dielectric function that is valid for all CZTSSe solid solutions [$0 \leq x \leq 1$]. These results are relevant for the design of efficient kesterite-based photovoltaic devices with an improved absorption range. The understanding of the influence of the content of S on the optical properties of kesterite materials opens the way to the development of efficient band gap graded photovoltaic devices.

6. Acknowledgments

The research leading to the presented results was partially supported by the European Project INFINITE-CELL (Ref. H2020-MSCA-RISE-2017-777968, 2017–2021, www.infinitecell.eu) and the Spanish MINECO Projects “WINCOST” (ENE2016-80788-C5-2-R) and "SENSIL" RTI2018-096498-B-I00 (MCIU/AEI/FEDER, UE). The authors from the Institute of Applied Physics appreciate the financial support from the Bilateral Project No. ANCD 19.80013.16.02.01F/BL and from the Institutional Project No. CSSDT 15.817.02.04A. Authors from IREC belong to the M-2E (Electronic Materials for Energy) Consolidated Research Group and the XaRMAE Network of Excellence on Materials for Energy of the "Generalitat de Catalunya". M. Guc This project has received funding from the European Union’s Horizon 2020 research and innovation programme under the Marie Skłodowska-Curie grant agreement No 712949 (TECNIOspring PLUS) and the Government of Catalonia's Agency for Business Competitiveness(ACCIÓ).

7. References

[1] S. Hood, A. Walsh, C. Persson, K. Iordanidou, D. Huang, M. Kumar, Z. Jehl, M. Courel, J. Lauwaert, S. Lee, Status of materials and device modelling for kesterite solar cells, J. Phys. Energy 1(4) (2019) 042004/1–8.

[2] S. Schorr, G. Gurieva, M. Guc, M. Dimitrievska, A. Pérez-Rodríguez, V. Izquierdo-Roca, C.S. Schnohr, J. Kim, W. Jo, J.M. Merino, Point defects, compositional fluctuations and secondary phases in non-stoichiometric kesterites, J. Phys. Energy 2(1) (2019) 012002/1–40.

[3] M. Grossberg, J. Krustok, C.J. Hages, D. Bishop, O. Gunawan, R. Scheer, S.M. Lyam, H. Hempel, S. Levcenko, T. Unold, The electrical and optical properties of kesterites, J. Phys. Energy 1 (2019) 044002/1–16.

[4] S. Chen, A. Walsh, X.-G. Gong, Su-H. Wei, Classification of lattice defects in the kesterite Cu_2ZnSnS_4 and $Cu_2ZnSnSe_4$ earth-abundant solar cell absorbers. Adv. Mater., 25 (2013) 1522-1539.

[5] W. Wang, M.T. Winkler, O.Gunawan, T. Gokmen, T.K. Todorov, Yu Zhu, D.B. Mitzi, Device characteristics of CZTSSe thin-film solar cells with 12.6% efficiency, Adv. Energy Mater. 4(7) (2013) 1301465/1–5.

[6] M. Dimitrievska, H. Xie, A. Fairbrother, X. Fontané, G. Gurieva, E. Saucedo, A. Pérez-Rodríguez, S. Schorr, and V. Izquierdo-Roca, Multiwavelength excitation Raman scattering of $Cu_2ZnSn(S_xSe_{1-x})_4$ $(0 \leq x \leq 1)$ polycrystalline thin films: Vibrational properties of sulfoselenide solid solutions, Appl. Phys. Lett. 105 (2014) 031913/1–5.

[7] G. Gurieva, M. Dimitrievska, S. Zander, A. Pérez-Rodríguez, V. Izquierdo-Roca, S. Schorr, Structural characterisation of $Cu_{2.04}Zn_{0.91}Sn_{1.05}S_{2.08}Se_{1.92}$. Phys. Status Solidi C 12(6) (2015) 588–591 (2015).

[8] M. Dimitrievska, G. Gurieva, H. Xie, A. Carrete, A. Cabot, E. Saucedo, A. Pérez-Rodríguez, S. Schorr, V. Izquierdo-Roca, Raman scattering quantitative analysis of the anion chemical composition in kesterite $Cu_2ZnSn(S_xSe_{1-x})_4$ solid solutions, J. Alloys Compd. 628 (2015) 464–470.

[9] A. Khare, B. Himmetoglu, M. Cococcioni, and E.S. Aydil, First principles calculation of the electronic properties and lattice dynamics of $Cu_2ZnSn(S_{1-x}Se_x)_4$, J. Appl. Phys. 111 (2012) 123704/1–8.

[10] E. Garcia-Llamas, M. Guc, I.V. Bodnar, X. Fontané, R. Caballero, J.M. Merino, M. León, V. Izquierdo-Roca, Multiwavelength excitation Raman scattering of $Cu_2ZnSn_{1-x}Gex(S,Se)_4$ single crystals for earth abundant photovoltaic applications, J. Alloys Compd. 692 (2017) 249–256.

[11] P. Bais, M. Teresa Caldes, M. Paris, C. Guillot-Deudon, P. Fertey, B. Domengès, A. Lafond, Cationic and Anionic Disorder in CZTSSe Kesterite Compounds: A Chemical Crystallography Study, Inorg. Chem. 56 (2017) 11779–11786.

[12] I.V. Bodnar, On the band gap of $Cu_2ZnSn(S_xSe_{1-x})_4$ alloys, Semiconductors 49, (2015) 1145-1148.

[13] S.Y. Li, S. Zamulko, C. Persson, N. Ross, J.K. Larsen, C. Platzer-Björkman, Optical properties of $Cu_2ZnSn(S_xSe_{1-x})_4$ solar absorbers: Spectroscopic ellipsometry and ab initio calculations, Appl. Phys. Lett. 110 (2017) 021905/1–5.

[14] S. Y. Li, C. Hägglund, Y. Ren, J.J. Scragg, J.K. Larsen, C. Frisk, K. Rudisch, S. Englund, and C. Platzer-Björkmann, Optical properties of reactively sputtered Cu_2ZnSnS_4 solar absorbers determined by spectroscopic ellipsometry and spectrophotometry, Sol. Energy Mater. Sol. Cells 149 (2016) 170–178.

[15] S. Zamulko, K. Berland, and C. Persson, Optical properties of $Cu_2ZnSn(S_xSe_{1-x})_4$ by first-principles calculations, Phys. Status Solidi A 215 (2018) 1700945/1–7.

[16] Z.-Y. Zhao, Q.-L. Liu, X. Zhao, DFT calculations study of structural, electronic, and optical properties of $Cu_2ZnSn(S_{1-x}Se_x)_4$ alloys, J. Alloys Compd. 618 (2015) 248–253.

[17] M. León, S. Levcenko, R. Serna, I.V. Bodnar, A. Nateprov, M. Guc, G. Gurieva, N. Lopez, J.M. Merino, R. Caballero, S. Schorr, A. Perez-Rodriguez, and E. Arushanov, Spectroscopic ellipsometry study of $Cu_2ZnSnSe_4$ bulk crystals, Appl. Phys. Lett. 105 (2014) 061909/1–4.

[18] J.G. Albornoz, R. Serna, and M. Leon, Optical properties and electronic structure of polycrystalline $Ag_{1-x}Cu_xInSe_2$ alloys, J. Appl. Phys. 97 (2005) 103515/1–7.

[19] T. Kawashima, S. Adachi, H. Miyake, and K. Sugiyama, Optical constants of $CuGaSe_2$ and $CuInSe_2$, J. Appl. Phys. 84 (1998) 5202–5209.

[20] S. Adachi, T. Kimura, and N. Suzuki, Optical properties of CdTe: Experiment and modeling

J. Appl. Phys. 74 (1993) 3435.

[21] S. Levcenko, E. Hajdeu-Chicarosh, E. Garcia-Llamas, R. Caballero, R. Serna, I.V Bodnar, I.A Victorov, M. Guc, J. M. Merino, A. Pérez-Rodriguez, E. Arushanov, M. León, Spectroscopic ellipsometry study of Cu_2ZnSnS_4 bulk poly-crystals, Appl. Phys. Lett. 112 (2018) 161901/1–5.

[22] C.C. Kim, J.W. Garland, H. Abad, and P.M. Raccah, Modeling the optical dielectric function of semiconductors: Extension of the critical-point parabolic-band approximation, Phys. Rev. B 45 (1992) 11749.

[23] J. Humlíček , "Polarized light and Ellipsometry", pp. 3-90, in Handbook of Ellipsometry, H.G. Tompkins, and E.A. Irene Editors, William Andrew Publishing (2005) 891 p, ISBN: 0-8155-1499-9.

[24] S.H. Han, C. Persson, F.S. Hasoon, H.A. Al-Thani, A.M. Hermann, and D.H. Levi, Optical properties and electronic structures of $(4CuInSe2)_y(CuIn5Se8)_{1-y}$, Phys. Rev. B 74 (2006) 08521.

[25] M. Erman, J.B. Theeten, P. Chambon, S.M. Kelso, and D.E. Aspnes, Optical properties and damage analysis of GaAs single crystals partly amorphized by ion implantation, J. Appl. Phys. 56 (1984) 2664–2671.

[26] A. Corana, M. Marchesi, C. Martini, and S. Ridella, Minimizing Multimodal Functions of Continuous Variables with the "Simulated Annealing" Algorithm, ACM T.Math. Software 13 (1987) 262–280.

[27] A.B. Djurišić, and E.H. Li, Modeling the optical constants of hexagonal GaN, InN, and AlN, J. Appl. Phys. 85 (1999) 2848–2853.

[28] G.E. Jellison, Jr., "Data Analysis for Spectroscopic Ellipsometry", pp. 237-296, in Handbook of Ellipsometry, H.G. Tompkins, and E.A. Irene Editors, William Andrew Publishing (2005) 891 p, ISBN: 0-8155-1499-9.

[29] K. Nagaya, S. Fujimoto, H. Tampo, S. Kim , M. Nishiwaki, Y. Nishigaki, M. Kato, H. Shibata, and H. Fujiwara, Very small tail state formation in $Cu_2ZnGeSe_4$, Appl. Phys. Lett. 113(9) (2018) 093901/1–5.

[30] S. Ozaki, K. Hoshina, and Y. Usami, Optical properties and electronic energy-band structure of Cu_2ZnSnS_4, Phys. Status Solidi C 12 (2015) 717–720.

[31] J. Li, H. Du, J. Yarbrough, A. Norman, K. Jones, G. Teeter, F.L. Terry, and D. Levi, Spectral optical properties of Cu_2ZnSnS_4 thin film between 0.73 and 6.5 eV, Opt. Express 20(S2) (2012) A327–A332.

[32] S.G. Choi, H. Y. Zhao, C. Persson, C.L. Perkins, A.L. Donohue, B. To, A.G. Norman, J. Li, and I.L. Repins, Dielectric function spectra and critical-point energies of $Cu_2ZnSnSe_4$ from 0.5 to 9.0 eV, J. Appl. Phys. 111 (2012) 033506/1–6.

[33] L. de la Cueva, Y. Sánchez, L. Calvo-Barrio, F. Oliva, V. Izquierdo-Roca, S. Khelifi, T. Bertram, J.M. Merino, M. León, R. Caballero, Sulfurization of co-evaporated $Cu_2ZnSnSe_4$ thin film solar cells: The role of Na, Sol. Energy Mater. Sol. Cells 186 (2018) 115–123.

[34] C. Cai, S.-Y. Wei, W.-C. Huang, C.-H. Hsu, W.-H. Ho, C.-H. Lai, Efficiency enhancement of $Cu_2ZnSn(S,Se)_4$ solar cells by S-modified surface layers, Sol. Enery Mater. Sol. Cells 162 (2017) 21–29.

[35] J. He, L. Sun, S. Chen, Y. Chen, P. Yang, J. Chu, Composition dependence of structure and optical properties of $Cu_2ZnSn(S,Se)_4$ solid solutions: An experimental study, J. Alloys Compd. 511 (2012) 129–132.